Petroleum Science 20 (2023) 1895–1902

Contents lists available at ScienceDirect

Petroleum Science

journal homepage: www.keaipublishing.com/en/journals/petroleum-science

Original Paper

Chelators to assist the high dispersion of Ni_2P particles over mesoporous silica nanospheres for hydrogenating reaction

Di Hu, En-Hua Wang, Ao-Cheng Wang, Ai-Jun Duan*

State Key Laboratory of Heavy Oil Processing, China University of Petroleum-Beijing, Beijing, 102249, China

ARTICLE INFO

Article history:
Received 13 July 2022
Received in revised form
12 August 2022
Accepted 21 November 2022
Available online 24 November 2022

Edited by Jia-Jia Fei

Keywords:
Wrinkle silica nanoparticles
Chelators
Ni_2P supported catalysts
Naphthalene hydrogenation

ABSTRACT

Ni_2P supported catalysts exhibit high catalytic activities in hydrogenation reaction, of which the particle sizes of Ni_2P active phases are the key influential factor. This research focus on the effect of chelators on the size of Ni_2P particles over wrinkle silica nanoparticles (WSNs) by introducing chelating agents EDTA and NTA during impregnation process. The characterization results show that chelators modified catalysts possess smaller size of Ni_2P particles than the unmodified Ni_2P catalysts. Among all the synthesized catalysts, the EDTA modified $Ni_2PE(1.5)$/WSNs catalyst possesses smallest average particle size of Ni_2P, only 2.6 nm. Moreover, the Ni_2P catalysts with the assistance of EDTA exhibits better catalytic activity than that of NTA under high reaction temperature, which can be ascribed to the strong bonding between EDTA and Ni. And the EDTA modified $Ni_2PE(1.5)$/WSNs catalyst shows highest hydrogenation ability, almost reaching 100% decalin selectivity.

© 2022 The Authors. Publishing services by Elsevier B.V. on behalf of KeAi Communications Co. Ltd. This is an open access article under the CC BY-NC-ND license (http://creativecommons.org/licenses/by-nc-nd/4.0/).

1. Introduction

Coal tar, as a main by-product in the process of coal pyrolysis, contains a large number of aromatic hydrocarbons (mainly bicyclic and tricyclic aromatic hydrocarbons) (Ardakani and Smith, 2011; Hodoshima et al., 2003; Liang et al., 2009; Zhao et al., 2010). The aromatics in low temperature coal tar can be converted into hydrogenated aromatics or cycloalkanes through catalytic hydrogenation, which can be used as the ideal component of jet fuel (Kim et al., 2017; Martin et al., 2020). Therefore, how to obtain high performance aromatic hydrogenation catalyst is the key to produce environmental-friendly fuels.

At present, transition metal sulfide catalysts are the main commercial catalysts for aromatic hydrogenation. Although they possess certain anti-poisoning ability, its hydrogenation activity is relatively low (Hart et al., 2020; Jing et al., 2020; Ohta et al., 1999). Noble metal catalysts show excellent hydrogenation saturation ability, but the high cost and easily poisoned by heteroatomic compounds containing S and N have restricted their industrial application (Tao et al., 2013; Zeng et al., 2018). In recently researches, transition metal carbides, transition metal nitrides and transition metal phosphides show great potential in the field of aromatic hydrogenation (Dongil, 2019; Prats et al., 2019; Zhang et al., 2019). More importantly, transition metal phosphide catalysts not only possess high hydrogenation activity, but also exhibit anti-toxicity ability (Usman et al., 2015). Among all phosphide catalysts, Ni_2P catalysts show high intrinsic hydrogenation activity due to its unique crystal morphology and electronic structure, which is expected to become a new generation of efficient aromatic hydrogenation catalyst (Oyama, 2003; Oyama and Lee, 2008; Zhao et al., 2020). However, the unsupported Ni_2P catalysts have the problems of small specific surface area, poor dispersion of active phase, low mechanical strength and poor heat dissipation, which are unfavorable to its hydrogenation activity. Therefore, researchers usually load the Ni_2P active components on various supports so as to expose more active sites and enhance hydrogenating activity.

As to the supported Ni_2P catalysts, the properties of different supports have an important effect on the dispersion of Ni_2P particles (Oyama and Lee, 2008). In recent years, compared with the traditional mesoporous silica nanoparticles, wrinkle silica nanospheres (WSNs) has attracted rapid attention due to its unique three-dimensional central-radial pore channels (Polshettiwar et al., 2011; Thankamony et al., 2015). Up to now, WSNs has a wide range of applications, such as catalysis, biotherapy delivery, water treatment, dye-sensitized solar cells, supercapacitors, fluorescent probes, titanium dioxide capture, and biological imaging,

* Corresponding author.
E-mail address: duanaijun@cup.edu.cn (A.-J. Duan).

https://doi.org/10.1016/j.petsci.2022.11.017
1995-8226/© 2022 The Authors. Publishing services by Elsevier B.V. on behalf of KeAi Communications Co. Ltd. This is an open access article under the CC BY-NC-ND license (http://creativecommons.org/licenses/by-nc-nd/4.0/).

photonics, composite materials, etc. Singh and Polshettiwar found that WSNs materials showed better textural stability, thermal stability and CO_2 capture capacity than the traditional mesoporous MCM-41 due to its unique fibrous morphology (Singh and Polshettiwar, 2016).

In order to improve the activity of the catalyst, scientific researchers focus on the introduction of organic complexing agents in the preparation of hydrogenation catalysts. Thomson R firstly introduced nitrilotriacetic acid (NTA) into NiMo/SiO_2 catalyst during impregnation process (Thompson, 1986). The hydrogenation denitrification (HDN) activity of NTA modified NiMo/SiO_2 catalyst was found to be 6 times higher than that of the traditional NiMo/SiO_2 catalyst without complexing agents. After that, many complexing agents, such as citric acid (CA), ethylene glycol (EG), nitrilotriacetic acid (NTA), ethylenediamine tetraacetic acid (EDTA), cyclohexylenediamine tetraacetic acid (CYDTA) and ethylenediamine (EN), were widely applied to the preparation of hydrogenation catalysts (Ding et al., 2017; Garcia-Ortiz et al., 2020; Jiang et al., 2020; Li et al., 2021; Santolalla-Vargas et al., 2020). Furthermore, Oyama and his groups found that small sizes of Ni_2P particles could expose more Ni(2) sites, thus enhancing the hydrogenation activity (Zhao et al., 2015; Shu et al., 2005). However, researches on the synthesis of small Ni_2P particles over the supported catalysts, especially less than 5 nm, are still limited. Therefore, the goal of this research is to synthesize small sizes of Ni_2P particles supported on the wrinkle silica nanoparticles.

In this study, the series of Ni_2P/WSNs catalysts were prepared by introducing chelators EDTA or NTA during the impregnation process. And the corresponding effects of chelators NTA and EDTA to Ni_2P/WSNs catalysts were also studied. The reaction of naphthalene hydrogenation was used to evaluate the catalytic activity and stability of chelators modified Ni_2P catalysts.

2. Experimental section

2.1. Synthesis of WSNs support

The WSNs material was synthesized as mentioned in the previous papers (Hu et al., 2019). 10 g CTAB and 6 g urea were dissolved in 300 mL distilled water and 300 mL cyclohexane. After complete dissolution, 40 mL TEOS was added dropwise. Then the mixture was continuously stirred for 24 h under 70 °C. The WSNs products were obtained by centrifugation, desiccation and calcination at 550 °C for 6 h.

2.2. Synthesis of Ni_2P/WSNs catalysts

The supported Ni_2P/WSNs catalysts were prepared by impregnation process and temperature-programmed reduction (TPR). The oxidic Ni_2P/WSNs catalyst precursors were obtained via a two-step incipient wetness method impregnated with aqueous solutions of nickel nitrate ($Ni(NO_3)_2\cdot 6H_2O$) and ammonium hypophosphite ($NH_4H_2PO_4$). After each impregnation, the catalyst was dried at 100 °C for 12 h and then calcined at 550 °C kept for another 3 h. The precursors were reduced at continuous H_2 flow rate of 150 mL min^{-1} and temperature of 440 °C kept for 1 h, then rising to 550 °C.

2.3. Synthesis of Ni_2PE/WSNs catalysts

The EDTA modified Ni_2PE/WSNs catalysts were prepared similar to the above process. Firstly, WSNs sample was impregnated with the aqueous mixed solutions of nickel nitrate ($Ni(NO_3)_2\cdot 6H_2O$) and EDTA. After dried at 100 °C for 12 h and then calcined at 550 °C for 3 h, the oxidic catalyst precursors were obtained by impregnating with ammonium hypophosphite ($NH_4H_2PO_4$). The molar ratios of Ni:P:EDTA were 1:1:0.5, 1:1:1 and 1:1:1.5, then the corresponding catalysts were named as $Ni_2PE(0.5)$/WSNs, $Ni_2PE(1.0)$/WSNs, and $Ni_2PE(1.5)$/WSNs respectively. Finally, the Ni_2PE/WSNs catalysts were collected by the same TPR progress.

2.4. Synthesis of Ni_2PN/WSNs catalysts

The NTA modified Ni_2PN/WSNs catalysts were prepared similar to the above Ni_2PE/WSNs process. The oxidic Ni_2PN/WSNs catalyst precursors were obtained by a two-step incipient wetness method with the mixed solution of nickel nitrate ($Ni(NO_3)_2\cdot 6H_2O$) and NTA, and ammonium hypophosphite ($NH_4H_2PO_4$). After each impregnation, the catalyst was dried at 100 °C for 12 h and then calcined at 550 °C kept for another 3 h. The synthesized catalysts were named as $Ni_2PN(0.5)$/WSNs, $Ni_2PN(1.0)$/WSNs, and $Ni_2PN(1.5)$/WSNs with different molar ratios of Ni:P:NTA (1:1:0.5, 1:1:1, 1:1:2). Finally, the Ni_2PN/WSNs catalysts were collected by the same TPR progress.

2.5. Measurement and characterization

Wide-angle X-ray diffraction patterns were collected on a Japan Shimadzu X-6000 system (Cu Ka radiation, 40 kV, 30 mA, $\lambda = 0.1540598$ nm). X-ray photoelectron spectroscopy (XPS) analysis was conducted using a PerkinElmer PHI-1600 ESCA spectrometer. N_2 adsorption-desorption experiments were performed at 77 K after degassing samples in flowing N_2 at 350 °C for 4 h (using a Q Micromeritics Tristar 3020). The morphological features of the samples were characterized by scanning electron microscopy (SEM, Hitachi SU-8010, 5.0 kV). Transmission electron microscopy (TEM, Philips Tecnai G2 F20 S-TWIN, 300 kV). The size distributions of Ni_2P phases were counted by more than 300 Ni_2P particles from different images through high-resolution transmission electron microscopy. The average Ni_2P particles were calculated according to Eq. (1).

$$D_{\text{aver}} = \frac{\sum_{i=1}^{n} d_i}{n_i} \tag{1}$$

where d_i represents the size of each Ni_2P particle and n_i is the total number of Ni_2P particles.

2.6. Catalytic activity measurements

The naphthalene hydrogenation was carried out with a fixed bed reactor. In general, 1.0 g of Ni_2P supported catalysts were loaded in the middle of a stainless steel tube reactor with both ends filled with mesh quartz sands. Before the reaction, the synthesized oxidation precursor was reduced to the active nickel phosphide in H_2 (4 MPa) at a flow rate of 150 mL min^{-1} by heating from room temperature at a heating rate of 5 °C min^{-1} to a temperature range as maintaining at 120 °C for 1 h, then rising up to 440 °C for 1 h and 550 °C for another 3 h, finally followed by cooling to room temperature in the continued H_2 flow. The 5% naphthalene in cyclohexane was used as the model compound to access aromatic hydrogenation activity. The system was pressurized under the condition of 4 MPa, H_2/Oil volumetric ratio of 500 (v/v), liquid hourly space velocity (WHSV) of 10 h^{-1}. The catalysts were evaluated at 300–380 °C with an interval of 20 °C. The outlet stream was analyzed using gas chromatography-mass spectrometry (GC-MS).

The conversion of naphthalene can be expressed by Eq. (2):

$$\text{Naphthalene}(\%) = \frac{N_f - N_P}{N_P} \quad (2)$$

where the N_f is the mass fraction of naphthalene in the feedstock and N_p is the mass fraction of naphthalene in the products.

3. Results

3.1. Characterization results of catalysts

3.1.1. XRD characterization

The peaks at 40.8°, 44.6°, 47.3°, 54.2° and 72.7° are tracked in Fig. 1, which are attributed to the characteristic responses of Ni_2P (PDF 3–953) (Tang et al., 2017). It is found that the peak intensities of Ni_2P particles become gradually weak with the addition of chelating agents, which maybe be ascribed that Ni_2P particles on the catalyst surface are too small to be detected by XRD characterization (Pullan et al., 2016; Yang et al., 2006).

The XRD patterns of the spent catalysts are also characterized to test their stability. As shown in Fig. 1b, there is almost no change of the Ni_2P characteristic peaks and no other unrelated peaks are detected in XRD, which confirms the high stability of the series Ni_2P/WSNs catalysts after reaction.

3.1.2. N_2 adsorption-desorption characterization

The N_2 adsorption-desorption patterns of the synthesized catalysts after the addition of chelators are shown in Fig. 2a. It can be seen that all catalysts showed type IV isotherms, indicating the good mesoporous structure. Fig. 2b shows the pore size distribution of the modified Ni_2P/WSNs catalysts, and the results are summarized in Table 1. The surface area and average pore size of the catalysts modified with chelators EDTA and NTA increase to some extent compared to the unmodified catalysts, which indicates that chelators can effectively inhibit the aggregation of Ni_2P active phases.

3.1.3. TEM characterization

It can be seen in TEM images, all the catalysts still retain their original morphologies, which demonstrate that the addition of chelators has little damage to the morphology of the WSNs support. In addition, the morphologies of the spent catalysts after reaction are nearly the same as the fresh catalysts, as displayed in Fig. 3 and Fig. 4, further confirming the high stabilities of the chelators modified Ni_2P/WSNs catalysts.

The average particle sizes of Ni_2P can be statistically calculated from high resolution TEM images (Figs. S1 and S2), as summarized in Table 2. It can be found that the average Ni_2P particle sizes of Ni_2PE/WSNs and Ni_2PN/WSNs catalysts are both smaller than those of unmodified Ni_2P/WSNs catalysts. Moreover, Ni_2PE/WSNs catalysts modified by EDTA possess smaller sizes of Ni_2P particles compared with Ni_2PN/WSNs catalysts with the addition of NTA, confirming that the chelator EDTA plays a greater role in preventing Ni_2P aggregation than the chelator NTA.

3.1.4. H_2-TPR characterization

It can be seen from Fig. 5 that H_2-TPR patterns show several H_2 consumption peaks in the vicinity of 400 °C and 700 °C. The H_2 consumption peak near 400 °C is attributed to the reduction of NiO species (Louis et al., 1993), while the H_2 consumption peak near 700 °C is derived from the P species due to the high P—O bond energy (Zuzaniuk and Prins, 2003).

The reduction peak of Ni species is shifted to the higher temperature for the samples obtained with the addition of chelators, indicating that the interaction between Ni and support become stronger as the chelator EDTA or NTA being added. Meanwhile, the reduction temperature of P species over EDTA modified catalysts is shifted to slightly lower temperature, leading to the small reduction-peak interval of Ni and P species, thus promoting the formation of Ni_2P active phase.

3.1.5. XPS characterization

XPS was used to investigate the differences in the chemical states of Ni and P on the surface of Ni_2P supported catalysts. As can be seen from Fig. S3 and Table 3, there are two XPS peaks of Ni 2p at around 853.1 eV and 856.9 eV, which are caused by the $Ni^{\delta+}$ ($0 < \delta < 1$) species in Ni_2P and Ni^{2+} interacting with PO_4^{3-}, respectively.

Three P 2p XPS peaks appeared at the binding energy of about 129.5 eV, 133.5 eV and 134.5 eV (Fig. S4), which are assigned to $P^{\delta-}$ ($0 < \delta < 1$) in Ni_2P, P^{3+} in $H_2PO_3^-$ and P^{5+} in PO_4^{3-}, respectively. It can be found from Table 2, the supported Ni_2P catalysts modified with the chelators of ETDA and NTA exhibit much higher proportions of Ni_2P than the traditional Ni_2P/WSNs catalysts without chelator addition.

3.2. The results of naphthalene selective hydrogenation

Naphthalene is chosen as the model compound to investigate the aromatic hydrogenation activity of synthesized catalysts, and

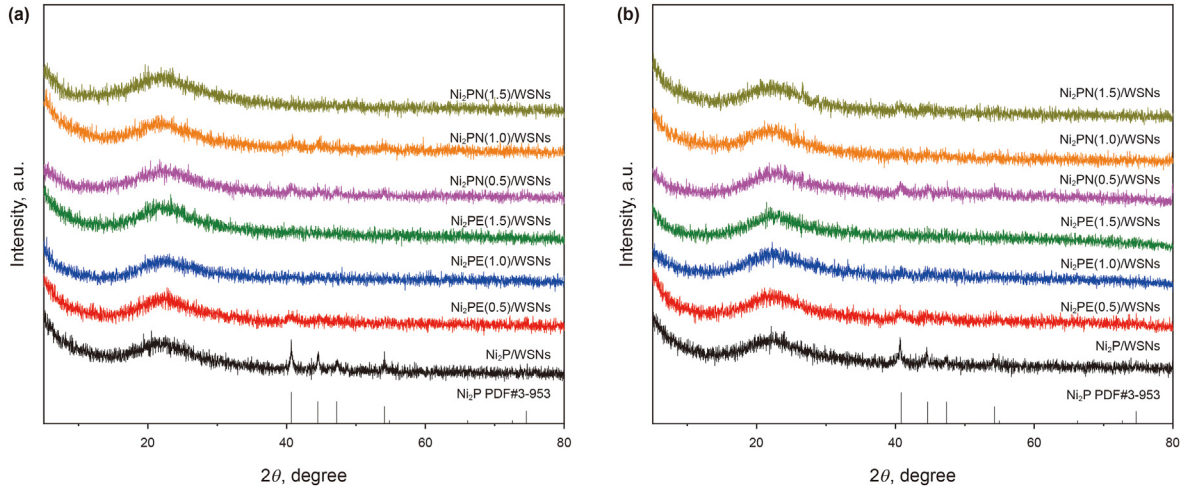

Fig. 1. XRD patterns of Ni_2PE/WSNs and Ni_2PN/WSNs series (**a**) fresh catalysts and (**b**) spent catalysts.

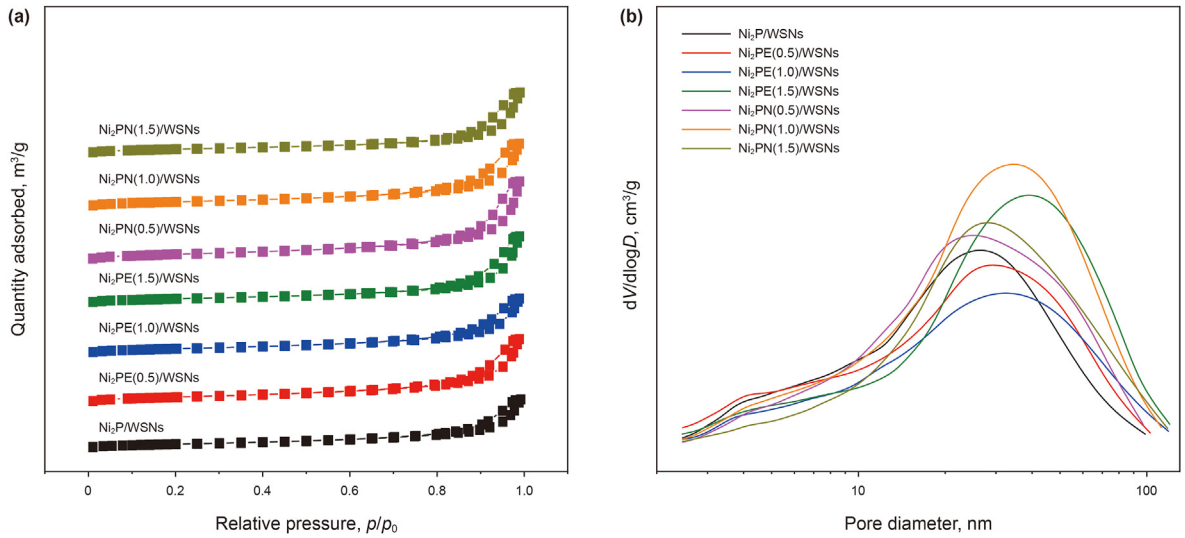

Fig. 2. (**a**) N_2 physisorption isotherms and (**b**) pore diameter distribution patterns of Ni_2PE/WSNs and Ni_2PN/WSNs series catalysts.

Table 1
Textural properties of Ni_2PE/WSNs and Ni_2PN/WSNs series catalysts.

Catalysts	S_{BET}, m^2/g[a]	V_t, cm^3/g[b]	D_{BJH}, nm[c]
Ni_2P/WSNs	117	0.49	13.9
$Ni_2PE(0.5)$/WSNs	156	0.49	13.3
$Ni_2PE(1.0)$/WSNs	160	0.44	16.1
$Ni_2PE(1.5)$/WSNs	161	0.66	18.6
$Ni_2PN(0.5)$/WSNs	133	0.56	15.7
$Ni_2PN(1.0)$/WSNs	154	0.70	17.0
$Ni_2PN(1.5)$/WSNs	184	0.54	18.6

[a] Surface area obtained by BET method.
[b] Total pore volume obtained by BET method.
[c] Pore diameter collected from the adsorption isotherm by BJH method.

the reaction pathway of naphthalene hydrogenation is displayed in Fig. S5. As shown in Fig. 6, the hydrogenation conversion of the EDTA and NTA modified catalysts are higher than that of supported Ni_2P catalysts without chelators. The decalin selectivity graph is shown in Fig. 7. In the experimental temperature range, EDTA-modified catalysts show high hydrogenation ability, among which $Ni_2PE(1.5)$/WSNs exhibits the highest decalin selectivity (almost reaching 100%). In the case of the NTA modified catalysts, high decalin selectivity of naphthalene is shown in temperature of 300 °C, but then decreases a lot when the reaction temperature enhances.

4. Discussion

4.1. Facilitation of small size Ni_2P particles formed on the supported catalysts by chelators addition

The Ni_2P supported series catalysts are successfully prepared on wrinkle silica nanoparticles (WSNs) support through temperature programmed reduction, which can be confirmed by the Ni_2P

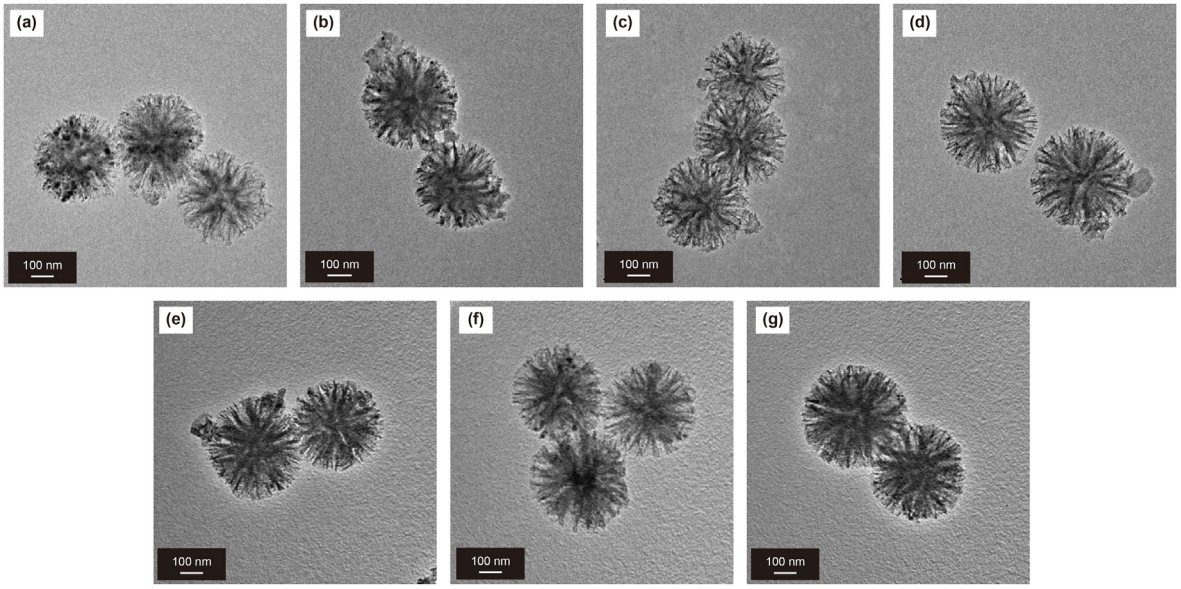

Fig. 3. TEM patterns of Ni_2PE/WSNs and Ni_2PN/WSNs series fresh catalysts. (**a**) Ni_2P/WSNs; (**b**) $Ni_2PE(0.5)$/WSNs; (**c**) $Ni_2PE(1.0)$/WSNs; (**d**) $Ni_2PE(1.5)$/WSNs; (**e**) $Ni_2PN(0.5)$/WSNs; (**f**) $Ni_2PN(1.0)$/WSNs; (**g**) $Ni_2PN(1.5)$/WSNs.

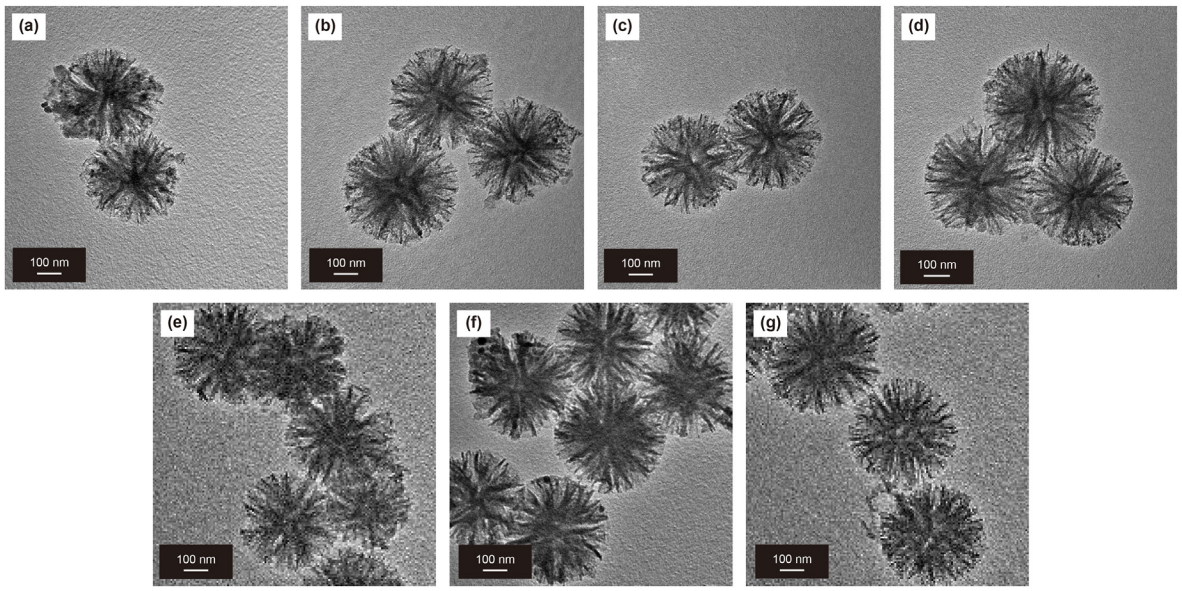

Fig. 4. TEM images of Ni_2PE/WSNs and Ni_2PN/WSNs series spent catalysts. (**a**) Ni_2P/WSNs; (**b**) $Ni_2PE(0.5)$/WSNs; (**c**) $Ni_2PE(1.0)$/WSNs; (**d**) $Ni_2PE(1.5)$/WSNs; (**e**) $Ni_2PN(0.5)$/WSNs; (**f**) $Ni_2PN(1.0)$/WSNs; (**g**) $Ni_2PN(1.5)$/WSNs.

Table 2
The average size of Ni_2P obtained by statistical analyses based on TEM images.

Samples	D_{aver}, nm
Ni_2P/WSNs	5.6
$Ni_2PE(0.5)$/WSNs	4.9
$Ni_2PE(1.0)$/WSNs	3.9
$Ni_2PE(1.5)$/WSNs	2.6
$Ni_2PN(0.5)$/WSNs	5.4
$Ni_2PN(1.0)$/WSNs	5.2
$Ni_2PN(1.5)$/WSNs	3.7

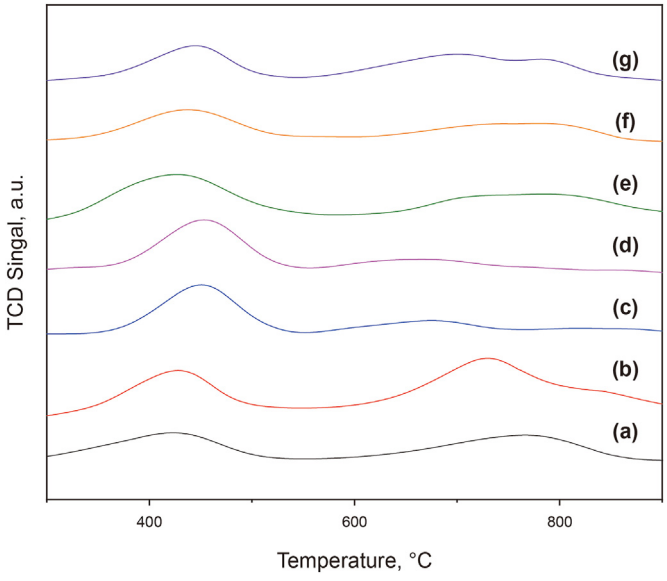

Fig. 5. H_2-TPR patterns of Ni_2PE/WSNs and Ni_2PN/WSNs series catalysts. (**a**) Ni_2P/WSNs; (**b**) $Ni_2PE(0.5)$/WSNs; (**c**) $Ni_2PE(1.0)$/WSNs; (**d**) $Ni_2PE(1.5)$/WSNs; (**e**) $Ni_2PN(0.5)$/WSNs; (**f**) $Ni_2PN(1.0)$/WSNs; (**g**) $Ni_2PN(1.5)$/WSNs.

characteristic peaks as shown on the XRD pattern. More importantly, the peaks of Ni_2P become broader and weaker as the addition of chelators, indicating that the corresponding sizes of Ni_2P also become smaller according to the Scherrer formula (Song et al., 2018). These results are in agreement with the TEM results, as shown in Table 1. The average sizes of Ni_2P particles decrease as the increasing addition of chelators. Among all the catalysts, $Ni_2PE(1.5)$/WSNs catalyst possesses the smallest Ni_2P average particle size of only 2.6 nm. The Ni_2P particle size obtained by the addition of EDTA and NTA in this work is smaller than the published works, realizing the formation of utral-small Ni_2P particles (Table S1). Previous reports (Rui and Smith, 2010; Zhang et al., 2017) have been reported that the chelators can form a metal complex with the active metals, so as to restrict the aggregation of metal specials on the supports. Therefore, the chelators have a positive effect on the formation of smaller Ni_2P particles on the supported catalysts.

4.2. Promotion the reduction of supported Ni_2P catalysts with the addition of chelators

The addition of chelator can contribute to the formation of Ni_2P active phase. As seen in XPS results, the Ni_2P proportion of the supported Ni_2P catalysts with the addition of EDTA and NTA is higher than that of Ni_2P/WSNs catalysts without chelators. More importantly, when the content of chelators is enhanced, the corresponding percentage of Ni_2P is also increased. Therefore, it can be speculated that EDTA and NTA chelators are beneficial to the reduction of Ni_2P, which can effectively avoid the generation of other impurity phase. Moreover, H_2-TPR results showed that the reduction-peak interval between Ni and P species becomes smaller as the addition of chelators, which further confirms the positive effect on the formation of Ni_2P active phase. During the H_2-TPR process, nickel species were first reduced and then H_2 dissociated from metallic Ni sites to form hydrogen spillover effects, which contributes to the reduction of the P species (Chen et al., 2010; Yang et al., 2013). The high dispersion of nickel species influenced by the chelator EDTA and NTA could have a chain effect on the later

Table 3
XPS analysis results of Ni_2PE/WSNs and Ni_2PN/WSNs series catalysts.

Catalysts	Ni $2p_{3/2}$ (binding energy)[a]		P $2p_{3/2}$ (binding energy)[a]		
	Ni^{2+}	Ni_2P	PO_4^{3-}	$H_2PO_3^-$	Ni_2P
Ni_2P/WSNs	857.0 (83.2)	853.5 (16.8)	134.4 (67.0)	133.5 (26.8)	129.0 (6.2)
$Ni_2PE(0.5)$/WSNs	856.9 (75.5)	853.1 (24.5)	134.5 (61.4)	133.5 (22.9)	129.5 (15.7)
$Ni_2PE(1.0)$/WSNs	856.9 (71.8)	853.4 (28.2)	134.2 (69.6)	133.1 (10.6)	129.5 (19.8)
$Ni_2PE(1.5)$/WSNs	856.8 (67.9)	853.2 (32.1)	134.3 (49.6)	133.3 (25.4)	129.4 (25.0)
$Ni_2PN(0.5)$/WSNs	856.7 (63.4)	853.2 (36.6)	134.8 (61.2)	133.8 (31.5)	129.1 (7.3)
$Ni_2PN(1.0)$/WSNs	857.2 (62.0)	853.5 (38.0)	135.2 (33.3)	134.2 (53.1)	129.5 (13.6)
$Ni_2PN(1.5)$/WSNs	856.9 (61.9)	853.1 (38.1)	134.7 (48.0)	133.4 (25.6)	129.5 (26.4)

[a] The data in parentheses are atom percentages.

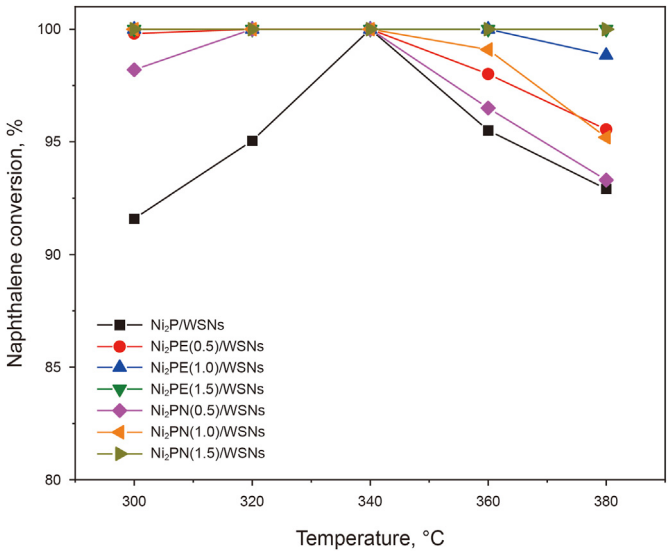

Fig. 6. Naphthalene conversion over Ni_2PE/WSNs and Ni_2PN/WSNs series catalysts.

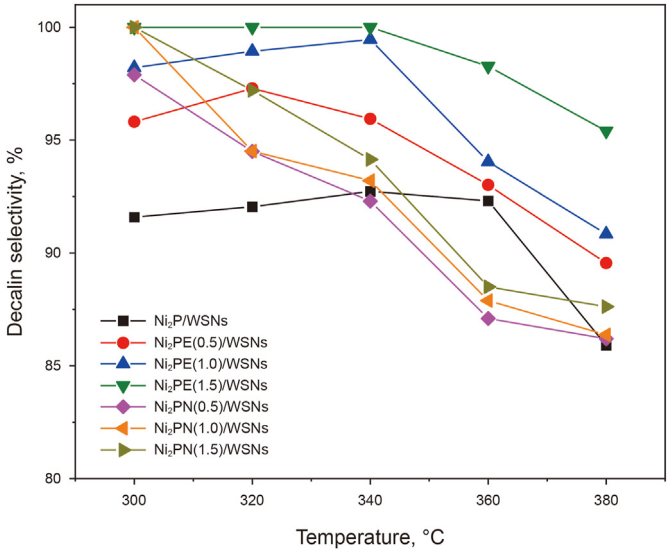

Fig. 7. The decalin selectivity of Ni_2PE/WSNs and Ni_2PN/WSNs series catalysts.

reduction of the P—O bond. Therefore, the better Ni dispersion of supported Ni_2P catalysts resulted from chelator additions are beneficial to the formation of nickel phosphide phases.

4.3. Different effects of chelators EDTA and NTA on the stability of the supported Ni_2P catalysts

On close observation of the structure of the chelating agent, it can be seen from Fig. 8 that there are four carboxyl groups and two nitrogen atoms in the case of EDTA, while there are only three carboxyl groups and one nitrogen atom with regard to NTA (Rufus et al., 2004). It is well known that Ni ion has a coordination number of six. When the Ni ion is bound to the chelator EDTA, all six ligand groups of the EDTA fill all the available coordination sites of Ni ion (Wang et al., 2002). However, four of the six coordination sites of Ni ion are occupied by the chelator NTA, leaving two free binding sites on the Ni ion (Lauer and Nolan, 2002). Therefore, Ni-EDTA complex is more stable compared with Ni-NTA complex since all coordination sites are involved in the formation of Ni-EDTA complex. In this case, the addition of EDTA can significantly reduce the interaction between Ni_2P and the support, thus forming relatively small Ni_2P particles with good dispersion.

The result of naphthalene hydrogenation can also reflect the different stabilities of the chelators EDTA and NTA, as shown in Fig. 7. The NTA modified catalysts exhibit high decalin selectivity under low temperature of 300 °C, which may be ascribed to the two free binding sites available on the Ni metal ion. However, the hydrogenation conversion of NTA modified catalyst decreases dramatically when the reaction temperature raises higher, while EDTA tailored catalysts still remain high stability under high temperature owing to all the coordination sites involved in the formation of complexation. The long-period (100 h) naphthalene hydrogenation experiments (Fig. S6) and XPS results of the spent $Ni_2PE(1.5)$/WSNs catalyst (Fig. S7 and Table S2) also shows that $Ni_2PE(1.5)$/WSNs catalyst possesses outstanding catalytic stabilities.

5. Conclusions

A facile strategy was developed for the preparation of the supported Ni_2P catalysts with small Ni_2P particles through the addition of chelators in this research. The reaction evaluation of naphthalene hydrogenation has shown that Ni_2P supported catalysts with the addition of EDTA and NTA chelators display higher catalytic activity than the traditional catalysts, among which $Ni_2PE(1.5)$/WSNs catalyst with the smallest Ni_2P particles nearly reaches 100% naphthalene conversion. Moreover, EDTA modified catalysts display high catalytic stability under high temperature due to the chelator EDTA completely bound to all coordination sites of Ni ions. On the contrary, NTA modified catalysts show high decalin selectivity on the temperature of 300 °C, but decrease a lot when the reaction temperature becomes higher due to the two free binding sites on the Ni ion.

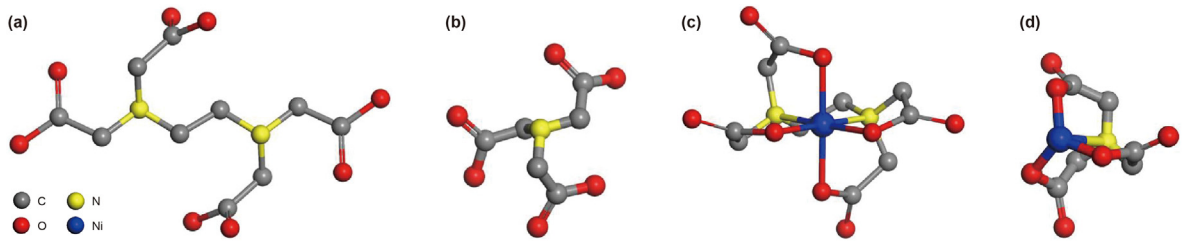

Fig. 8. Molecule structures of (**a**) EDTA and (**b**) NTA and (**c**) Ni-EDTA complex and (**d**) Ni-NTA complex. The hydrogen atom was hidden.

Declaration of competing interest

The authors declare that they have no known competing financial interests or personal relationships that could have appeared to influence the work reported in this paper.

Acknowledgments

This research is financially supported by the National Natural Science Foundation of China (No. 21878330), Key Research and Development Program of Ministry of Science and Technology of China (No. 2019YFC1907602) and Scientific Research and Technology Development Program of China National Petroleum Corporation (2020B-2116).

Appendix A. Supplementary data

Supplementary data to this article can be found online at https://doi.org/10.1016/j.petsci.2022.11.017.

References

Ardakani, S.J., Smith, K.J., 2011. A comparative study of ring opening of naphthalene, tetralin and decalin over Mo2C/HY and Pd/HY catalysts. Appl. Catal. Gen. 403 (1–2), 36–47. https://doi.org/10.1016/j.apcata.2011.06.013.

Chen, J., Chen, Y., Yang, Q., et al., 2010. An approach to preparing highly dispersed Ni_2P/SiO_2 catalyst. Catal. Commun. 11 (6), 571–575. https://doi.org/10.1016/j.catcom.2009.12.022.

Ding, J., Popa, T., Tang, J., et al., 2017. Highly selective and stable Cu/SiO_2 catalysts prepared with a green method for hydrogenation of diethyl oxalate into ethylene glycol. Appl. Catal. B Environ. 209, 530–542. https://doi.org/10.1016/j.apcatb.2017.02.072.

Dongil, A.B., 2019. Recent progress on transition metal nitrides nanoparticles as heterogeneous catalysts. Nanomaterials 9 (8), 1111–1128. https://doi.org/10.3390/nano9081111.

Garcia-Ortiz, A., Vidal, J.D., Iborra, S., et al., 2020. Synthesis of a hybrid Pd^0/Pd-carbide/carbon catalyst material with high selectivity for hydrogenation reactions. J. Catal. 389, 706–713. https://doi.org/10.1016/j.jcat.2020.06.036.

Hart, A., Adam, M., Robinson, J.P., et al., 2020. Hydrogenation and dehydrogenation of tetralin and naphthalene to explore heavy oil upgrading using $NiMo/Al_2O_3$ and $CoMo/Al_2O_3$ catalysts heated with steel balls via induction. Catalysts 10 (5), 497–514. https://doi.org/10.3390/catal10050497.

Hodoshima, S., Arai, H., Takaiwa, S., et al., 2003. Catalytic decalin dehydrogenation/naphthalene hydrogenation pair as a hydrogen source for fuel-cell vehicle. Int. J. Hydrogen Energy 28 (11), 1255–1262. https://doi.org/10.1016/S0360-3199(02)00250-1.

Hu, D., Duan, A., Xu, C., et al., 2019. Ni_2P promotes the hydrogenation activity of naphthalene on wrinkled silica nanoparticles with tunable hierarchical pore sizes in a large range. Nanoscale 11 (33), 15519–15529. https://doi.org/10.1039/C9NR02597A.

Jiang, H., Lin, J., Wu, X., et al., 2020. Efficient hydrogenation of CO_2 to methanol over Pd/In_2O_3/SBA-15 catalysts. J. CO2 Util. 36, 33–39. https://doi.org/10.1016/j.jcou.2019.10.013.

Jing, J., Yanf, Z., Wang, J., et al., 2020. Effect of preparation methods on the structure and naphthalene hydrogenation performance of Ni_2P/SiO_2 catalyst. J. Fuel Chem. Technol. 48 (7), 842–851. https://doi.org/10.1016/S1872-5813(20)30058-X.

Kim, Y.S., Cho, K.S., Lee, Y.K., 2017. Morphology effect of β-zeolite supports for Ni2P catalysts on the hydrocracking of polycyclic aromatic hydrocarbons to benzene, toluene, and xylene. J. Catal. 351, 67–78. https://doi.org/10.1016/j.jcat.2017.03.006.

Lauer, S.A., Nolan, J.P., 2002. Development and characterization of Ni-NTA-bearing microspheres. Cytometry: J. Int. Soc. Anal. Cytol. 48 (3), 136–145. https://doi.org/10.1002/cyto.10124.

Li, Y., Men, Y., Liu, S., et al., 2021. Remarkably efficient and stable Ni/Y_2O_3 catalysts for CO_2 methanation: effect of citric acid addition. Appl. Catal. B Environ. 293, 120206–120216. https://doi.org/10.1016/j.apcatb.2021.120206.

Liang, C., Zhao, A., Zhang, X., et al., 2009. CoSi particles on silica support as a highly active and selective catalyst for naphthalene hydrogenation. Chem. Commun. Roy. Soc. Chem. 15, 2047–2049. https://doi.org/10.1039/B820519A.

Louis, C., Cheng, Z.X., Che, M., 1993. Characterization of nickel/silica catalysts during impregnation and further thermal activation treatment leading to metal particles. J. Phys. Chem. 97 (21), 5703–5712. https://doi.org/10.1021/j100123a040.

Martin, J., Knüpfer, C., Eyselein, J., et al., 2020. Highly active superbulky alkaline earth metal amide catalysts for hydrogenation of challenging alkenes and aromatic rings. Angew. Chem. Int. Ed. 59 (23), 9102–9112. https://doi.org/10.1002/ange.202001160.

Ohta, Y., Shimizu, T., Honma, T., et al., 1999. Effect of chelating agents on HDS and aromatic hydrogenation over CoMo- and NiW/Al_2O_3. Stud. Surf. Sci. Catal. 127, 161–168. https://doi.org/10.1016/S0167-2991(99)80405-4.

Oyama, S.T., 2003. Novel catalysts for advanced hydroprocessing: transition metal phosphides. J. Catal. 216 (1–2), 343–352. https://doi.org/10.1016/S0021-9517(02)00069-6.

Oyama, S.T., Lee, Y.K., 2008. The active site of nickel phosphide catalysts for the hydrodesulfurization of 4,6-DMDBT. J. Catal. 258 (2), 393–400. https://doi.org/10.1016/j.jcat.2008.06.023.

Polshettiwar, V., Thivolle-Cazat, J., Taoufik, M., et al., 2011. "Hydro-metathesis" of olefins: a catalytic reaction using a bifunctional single-site tantalum hydride catalyst supported on fibrous silica (KCC-1) nanospheres. Angew. Chem. Int. Ed. 50 (12), 2747–2751. https://doi.org/10.1002/anie.201007254.

Prats, H., Piñero, J.J., Viñes, F., et al., 2019. Assessing the usefulness of transition metal carbides for hydrogenation reactions. Chem. Commun. 55 (85), 12797–12800. https://doi.org/10.1039/C9CC06084G.

Pullan, L., Reynolds, M.A., Murray, B.D., et al., 2016. Highly-active nickel phosphide hydrotreating catalysts prepared in situ using nickel hypophosphite precursors. J. Catal. 335, 204–214. https://doi.org/10.1016/j.jcat.2015.12.006.

Rufus, A., Velmurugan, S., Sathyaseelan, V., et al., 2004. Comparative study of nitrilo triacetic acid (NTA) and EDTA as formulation constituents for the chemical decontamination of primary coolant systems of nuclear power plants. Prog. Nucl. Energy 44 (1), 13–31. https://doi.org/10.1016/S0149-1970(04)90005-4.

Rui, W., Smith, K.J., 2010. The effect of preparation conditions on the properties of high-surface area Ni_2P catalysts. Appl. Catal. Gen. 380 (1–2), 149–164. https://doi.org/10.1016/j.apcata.2010.03.055.

Santolalla-Vargas, C., Santes, V., Suarez-Toriello, V., et al., 2020. Effect of sulfidation pressure on the structure and activity of $Ni(CyDTA)W/\gamma\text{-}Al_2O_3$ hydrodesulfurization catalysts. Catal. Today 377, 92–99. https://doi.org/10.1016/j.cattod.2020.07.015.

Shu, Y., Lee, Y.K., Oyama, S.T., 2005. Structure-sensitivity of hydrodesulfurization of 4,6-dimethyldibenzothiophene over silica-supported nickel phosphide catalysts. J. Catal. 236 (1), 112–121. https://doi.org/10.1016/j.jcat.2005.08.015.

Singh, B., Polshettiwar, V., 2016. Design of CO_2 sorbents using functionalized fibrous nanosilica (KCC-1): insights into the effect of the silica morphology (KCC-1 vs. MCM-41). J. Mater. Chem. 4 (18), 7005–7019. https://doi.org/10.1039/C6TA01348A.

Song, H., Yu, Q., Jiang, N., et al., 2018. Effect of surface modification temperature on the hydrodesulfurization performance of Ni_2P/MCM-41 catalyst. Res. Chem. Intermed. 44 (5), 3629–3640. https://doi.org/10.1007/s11164-018-3329-9.

Tang, C., Zhang, R., Lu, W., et al., 2017. Energy-saving electrolytic hydrogen generation: Ni_2P nanoarray as a high-performance non-noble-metal Electrocatalyst. Angew. Chem. Int. Ed. 56 (3), 842–846. https://doi.org/10.1002/anie.201608899.

Tao, H., Wang, Y., Miao, P., et al., 2013. Hydrogenation of naphthalene over noble metal supported on mesoporous zeolite in the absence and presence of sulfur. Fuel 106, 365–371. https://doi.org/10.1016/j.fuel.2012.12.025.

Thankamony, A.S.L., Lion, C., Pourpoint, F., et al., 2015. Insights into the catalytic activity of nitridated fibrous silica (KCC-1) nanocatalysts from N^{15} and Si^{29} NMR spectroscopy enhanced by dynamic nuclear polarization. Angew. Chem. Int. Ed. 54, 2190–2193. https://doi.org/10.1021/acssuschemeng.5b00812.

Thompson, M., 1986. Preparation of High Activity Silica-Supported Hydrotreating Catalysts and Catalysts Thus Prepared. European Patent.

Usman, M., Li, D., Li, C., et al., 2015. Highly selective and stable hydrogenation of heavy aromatic-naphthalene over transition metal phosphides. Sci. China

Chem. 58 (4), 738–746. https://doi.org/10.1007/s11426-014-5199-3.
Wang, X., Clark, P., Oyama, S.T., 2002. Synthesis, characterization, and hydrotreating activity of several iron group transition metal phosphides. J. Catal. 208 (2), 321–331. https://doi.org/10.1006/jcat.2002.3604.
Yang, S., Liang, C., Prins, R., 2006. A novel approach to synthesizing highly active Ni_2P/SiO_2 hydrotreating catalysts. J. Catal. 237 (1), 118–130. https://doi.org/10.1016/j.jcat.2005.10.021.
Yang, Y., Chen, J., Shi, H., 2013. Deoxygenation of methyl laurate as a model compound to hydrocarbons on Ni_2P/SiO_2, Ni_2P/MCM-41, and Ni_2P/SBA-15 catalysts with different dispersions. Energy Fuel. 27 (6), 3400–3409. https://doi.org/10.1021/ef4004895.
Zeng, D., Xu, W., Ong, W.J., et al., 2018. Toward noble-metal-free visible-light-driven photocatalytic hydrogen evolution: monodisperse sub-15 nm Ni_2P nanoparticles anchored on porous g-C_3N_4 nanosheets to engineer 0D-2D heterojunction interfaces. Appl. Catal. B Environ. 221, 47–55. https://doi.org/10.1016/j.apcatb.2017.08.041.
Zhang, L., Fu, W., Yu, Q., et al., 2017. Effect of citric acid addition on the morphology and activity of Ni_2P supported on mesoporous zeolite ZSM-5 for the hydrogenation of 4, 6-DMDBT and phenanthrene. J. Catal. 345, 295–307. https://doi.org/10.1016/j.jcat.2016.11.019.
Zhang, X., Han, M., Liu, G., et al., 2019. Simultaneously high-rate furfural hydrogenation and oxidation upgrading on nanostructured transition metal phosphides through electrocatalytic conversion at ambient conditions. Appl. Catal. B Environ. 244, 899–908. https://doi.org/10.1021/jp9108706.
Zhao, A., Zhang, X., Xiao, C., et al., 2010. Cobalt silicide nanoparticles in mesoporous silica as efficient naphthalene hydrogenation catalysts by chemical vapor deposition. J. Phys. Chem. C 114 (9), 3962–3967. https://doi.org/10.1021/jp9108706.
Zhao, H., Oyama, S.T., Freund, H.J., et al., 2015. Nature of active sites in Ni_2P hydrotreating catalysts as probed by iron substitution. Appl. Catal. B Environ. 164, 204–216. https://doi.org/10.1016/j.apcatb.2014.09.010.
Zhao, S., Berry-Gair, J., Li, W., et al., 2020. The role of phosphate group in doped cobalt molybdate: improved electrocatalytic hydrogen evolution performance. Adv. Sci. 7 (12), 1903674–1903682. https://doi.org/10.1002/advs.201903674.
Zuzaniuk, V., Prins, R., 2003. Synthesis and characterization of silica-supported transition-metal phosphides as HDN catalysts. J. Catal. 219 (1), 85–96. https://doi.org/10.1016/S0021-9517(03)00149-0.